GEOPHYSICS, VOL. 70, NO. 2 (MARCH-APRIL 2005); P. F27–F33, 7 FIGS.
10.1190/1.1897030

Characterization of hydraulic properties of rocks using probability of fluid-induced microearthquakes

Serge A. Shapiro[1], Susanne Rentsch[1], and Elmar Rothert[1]

ABSTRACT

The use of borehole fluid injections is typical for exploration and development of hydrocarbon or geothermal reservoirs. Such injections often induce small-magnitude earthquakes. The nature of processes leading to triggering of such microseismicity is still not completely understood. Here, we consider induced microseismicity, using as examples two case studies of geothermal reservoirs in crystalline rocks and one case study of a tight-gas sandstone reservoir. In all three cases, we found that the probability of induced earthquakes occurring is very well described by the relaxation law of pressure perturbation in fluids filling the pore space in rocks. This strongly supports the hypothesis of seismicity triggered by pore pressure. Moreover, this opens additional possibilities of using passive seismic monitoring to characterize hydraulic properties of rocks on the reservoir scale with high precision.

INTRODUCTION

Injections of borehole fluids into surrounding rocks are used for development of hydrocarbon or geothermal reservoirs. Such injections often induce small-magnitude earthquakes (see, e.g., Zoback and Harjes, 1997, Fehler et al., 1998; Audigane et al., 2002; Rutledge and Phillips, 2003). The nature of such seismic activity is still under discussion (see, e.g., Trifu, 2002). Possible mechanisms of induced microseismicity are, for example, hydraulic fracturing or slip initiation by redistribution of elastic stress. Another widespread hypothesis explaining the phenomenon of hydraulically induced microseismicity (e.g., Nur and Booker, 1972; Pearson, 1981; Shapiro et al., 2002) is that the tectonic stress in the earth's crust at some locations is close to a critical stress causing brittle failure of rocks; for example, by sliding along preexisting cracks. Increasing fluid pressure in a reservoir causes pressure in the connected pore space of rocks to increase (the pore space includes pores, cracks, vicinities of grain contacts, and all other possible voids in rocks). This leads to an increase of pore pressure at the critical locations as well. Such an increase consequently causes a decrease of the effective normal stress, usually acting compressionally on arbitrary internal rock surfaces. This leads to sliding along preexisting, favorably oriented subcritical cracks.

The change of pore pressure in space and time is controlled by the diffusion process of pressure relaxation in fluids saturating the pores. Thus, if the hypothesis described above correctly explains at least one of the dominant mechanisms triggering fluid-induced microseismicity, then a number of diffusion-typical signatures should be observed in the spatiotemporal distributions of the earthquakes. Several of these signatures related to the temporal evolution of microseismicity clouds and supporting the above hypothesis are known, such as, for example, a parabolalike forward-triggering front and a back front of seismicity. Such fronts are visible on plots of event distances from the injection source versus their occurrence times (see, e.g., Audigane et al., 2002; Shapiro et al., 2003, Parotidis et al., 2004). Another diffusion-related signature is a convergence of seismicity clouds to ellipsoidlike figures by normalization of event coordinates by square roots of their occurrence times (see Shapiro et al., 2003). These signatures are related to the shape and size of seismicity clouds. In contrast to them, we report here evidence of a completely different nature supporting the hypothesis described above. This evidence is related to the spatial density of seismic events.

In the following, we propose a statistical model describing the probability of triggering microearthquakes. Then, we briefly describe how the data of microseismic monitoring should be processed in order to obtain useful information from the spatial density of the event distribution. Finally, using three case studies, we show that the theoretically predicted feature of the spatial density of events can be very well observed. Such a feature additionally illuminates the physics of

Manuscript received by the Editor September 25, 2003; revised manuscript received September 29, 2004; published online March 22, 2005.
[1]Freie Universität Berlin, Fachrichtung Geophysik, Malteserstrasse 74-100, 12249 Berlin, Germany. E-mail: shapiro@geophysik.fu-berlin.de; rentsch@geophysik.fu-berlin.de; rothert@geophysik.fu-berlin.de.
© 2005 Society of Exploration Geophysicists. All rights reserved.

the fluid-induced microseismicity. Moreover, it opens a new way to estimate hydraulic properties of natural rocks at large spatial scales with high precision.

STATISTICAL MODEL OF SEISMICITY TRIGGERING

We start with a theoretical model which is completely consistent with the above-described pore-pressure relaxation hypothesis (PRH). The assumptions of this model are the following: We consider a point pressure source in an infinite, homogeneous, permeable, porous continuum. We assume that the hydraulic diffusivity of this continuum is independent of position and time. As a result of fluid injection and the consequent process of pressure relaxation, the pore pressure p will change throughout the pore space. We assume that a critical value C of the pore pressure necessary for occurrence of a seismic event is randomly distributed in space. The statistical properties of C are assumed to be independent of position (i.e., $C(\mathbf{r})$ is a statistically homogeneous random field). If, at a given point $\mathbf{r}$ of the medium, pore pressure $p(t, \mathbf{r})$ increases with time, and at time t_0, it becomes equal to $C(\mathbf{r})$, then this point will be considered a hypocenter of an earthquake occurring at time t_0. For simplicity, we assume that no earthquake will be possible at this point again. Then, the probability of an earthquake occurring at a given point at a given time will be equal to $W[C(\mathbf{r}) \leq p(t, \mathbf{r})]$, which is the probability of the critical pressure being smaller than the pore pressure $p(t, \mathbf{r})$. If the pore pressure perturbation caused by the fluid injection is a nondecreasing function (which is the case for realistic, step-functionlike borehole-injection pressures), this probability will be equal to

$$W = \int_0^{p(t,\mathbf{r})} f(C)dC,$$

where $f(C)$ is the probability density function of the critical pressure. The pore pressure $p(t, \mathbf{r})$ is the solution of the diffusion equation describing the process of pore-pressure relaxation. According to this theoretical model, the seismic criticality of rocks is defined by the quantity C. If C is high, we speak about a stable domain of the medium. If C is low, we mean a seismic critical domain. Our experience with microseismic data shows that usually C is of the order of 10^2–10^5 Pa.

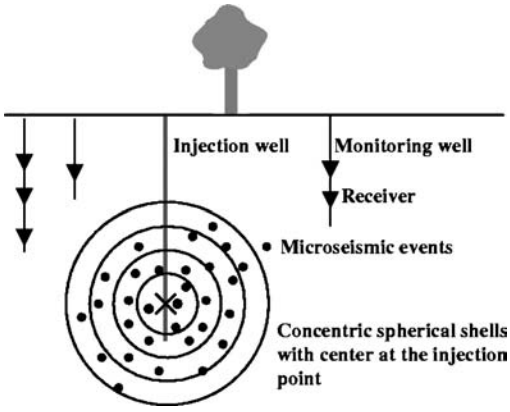

Figure 1. A sketch of possible acquisition and processing geometry for passive monitoring data. Multicomponent receivers can be located in several boreholes (Soultz case and Cotton Valley case) or in a single monitoring borehole. Receivers also can be placed on the earth surface (not shown here). The cross denotes the injection point. All other notations are explained in the figure.

The simplest possible distribution of the critical pore pressure is a uniform distribution $f = 1/A$, where A is a normalizing constant having the following physical meaning: $A = C_{\max} - C_{\min}$, with $C_{\max}$ and $C_{\min}$ standing for maximum and minimum possible critical pressures. In this case, $W = p(t, \mathbf{r})/A$, and the event probability is proportional to the pore-pressure perturbation. A question arises: is such a distribution of microearthquakes observed in reality? A positive answer to this question would be of significant importance for our understanding of the physics of microseismicity triggering as well as for useful applications of this phenomenon. Our observations provide such a positive answer.

PROCESSING OF PASSIVE MONITORING DATA

We consider several examples of borehole-fluid injections. The pore-pressure relaxation in a porous medium surrounding an injection source is described by the differential equation of diffusion. In many situations, realistic conditions of borehole-fluid injections can be approximated by a point pore-pressure source of constant strength q (this quantity has physical units of power) switched on at the time $t = 0$. The solution of the diffusion equation then has the following form [see Carslaw and Jaeger (1973), chapter 10.2 (2)]:

$$p = \frac{q}{4\pi Dr} \operatorname{erfc}\left(\frac{r}{\sqrt{4Dt}}\right). \tag{1}$$

Here, $\operatorname{erfc}(x)$ is the complementary Gaussian error function and t denotes observation time. The quantity D is an important hydraulic parameter of the rock, called hydraulic diffusivity. It is proportional to the darcy permeability K of rocks (Shapiro et al., 1999, 2002):

$$D = \frac{NK}{\eta}, \tag{2}$$

where η is the pore-fluid dynamic viscosity and N is a poroelastic modulus related to porosity, bulk modulus of fluid, and elastic moduli of the grain material and drained rock skeleton (see also Detournay and Cheng, 1993; Rice and Cleary, 1976; Van Der Kamp and Gale, 1983).

The event probability is proportional to the volumetric density of microseismic events. Therefore, a comparison of the volumetric event density of microseismicity clouds induced by fluid injections with equation 1 is required. Before we do this for a microseismic data set obtained during a real borehole-fluid injection, we consider a synthetic example.

Figure 1 shows a sketch of a passive-monitoring data acquisition. A synthetic cloud of microseismicity was obtained in a way consistent with the theory described above [such modeling was proposed and described by Rothert and Shapiro (2003)]. This cloud is shown at the left in Figure 2. The following processing can be proposed to compute the probabilities of seismic events occurring. We count the number of events in concentric spherical shells with the center at the injection point (see Figure 1). This number of events is assigned to the

mean radius of the corresponding shell. By normalizing event numbers to the shell volumes, we obtain the event density. We normalize the event densities by the event density in the second spherical shell in order to work with nondimensional quantities and to eliminate insignificant proportionality factors. (The first shell, which is actually a sphere around the injection point, is not considered because of the singularity of the diffusion-equation solution).

To compare these numerical results with predictions of equation 1, the analytical function $p(r, t)$ is also normalized by its value at the mean radius of the second spherical shell. Note that $p(r, t)$ is a function only of the radial distance from the injection point. Time in the Gaussian error function is the total period of the injection (which is also equal to the total period of observation, i.e., event counting). A very good agreement of the analytical curve calculated with a hydraulic diffusivity of $D = 1$ m^2/s and the event probability in the synthetic microseismic cloud (at the right in Figure 2) is not surprising. The numerical modeling is completely consistent with the PRH. The dashed line in Figure 2 was obtained using a 10% smaller hydraulic diffusivity and the dashed-dotted line using a 10% larger D. It should be noted that the observation time t (i.e., event-counting time) can be smaller than the total injection time. If t is too large, the normalized function $p(r, t)$ will become insensitive to D. On the other hand, if t is too small, the statistics of events can become insufficient for processing. In all synthetic examples and case studies given in this paper, the choice of t equal to the injection time is completely adequate.

In the case of real data, one more important complication must be taken into account. Hydraulic properties of natural rocks are usually anisotropic. Their hydraulic diffusivity is a second-rank tensor (Shapiro et al., 1999, 2002, 2003). If the PRH is valid, the geometry of the microseismic cloud should be controlled by this tensor (see Figure 3, left). In order to compare the spatial distribution of the event density with analytical solution 1, we have to transform the microseismic cloud obtained under pore-pressure relaxation in an anisotropic medium into a microseismic cloud which would be obtained in an isotropic medium. For this, a coordinate rotation is necessary from the original coordinate system (usually a geographic and depth-coordinate system of event locations) to a coordinate system oriented along the principal axes of the diffusivity tensor. In addition, after this rotation, the coordinates of events must be scaled in relation to the square roots of the corresponding principal values of the diffusivity tensor. Validity of this scaling procedure is a consequence of the equivalence of the diffusion equation in an isotropic medium to the diffusion equation in an anisotropic medium by the transformation of coordinates described above (see also, Carslaw and Jaeger, 1973, 38–43). The hydraulic diffusivity in the resulting isotropic-diffusion equation is equal to the arithmetic average of the principal components of the diffusivity tensor. A detailed description of this transformation for microseismic clouds and how to find the relationship between principal components of the hydraulic diffusivity tensor for real situations using microseismic clouds is given in Shapiro et al. (1999, 2003). Note that the algorithms of inversion for a diffusivity tensor described in these publications are able to provide orientations and relations between the tensor's principal components that are quite precise. However, their absolute values (i.e., the magnitude of the arithmetic average of the principal components) are estimated less precisely. This disadvantage can be compensated for by using the event probability analysis we describe here.

After the transformation of the seismicity cloud, a comparison between predictions of equation 1 and the event density is possible. It is completely analogous to the one in an isotropic medium. At the right in Figure 3, such a comparison is shown for the synthetic microseismicity on the left in Figure 3.

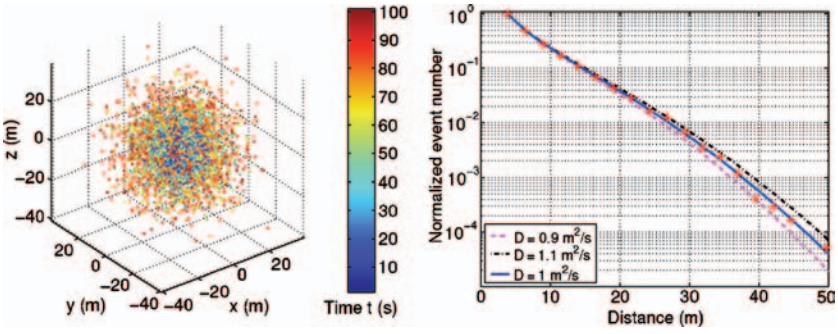

Figure 2. Synthetic microseismicity in a hydraulically isotropic model with the hydraulic diffusivity of 1 m^2/s. (Left) A view of the cloud of seismic events. The colors correspond to the event occurrence time in seconds. (Right) Spatial density of the microseismic cloud versus distance from the injection source (crosses). The lines denote the theoretical distribution given by equation 1.

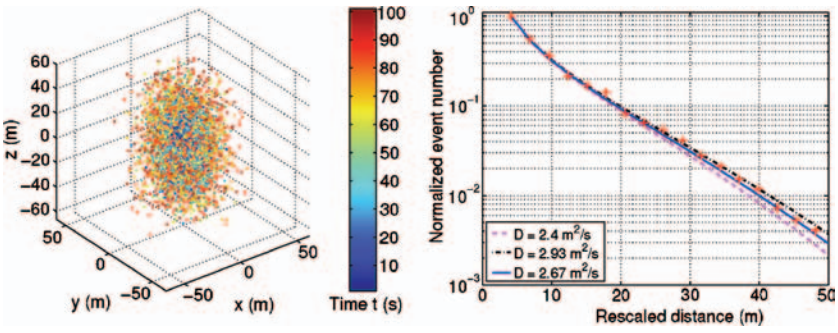

Figure 3. Synthetic microseismicity in a hydraulically anisotropic model. Principal components of the hydraulic diffusivity are 1 m^2/s, 2 m^2/s, and 5 m^2/s. Notations are as in Figure 2. (Left) A view of the cloud of seismic events. (Right) The spatial density of the microseismic cloud versus rescaled distance from the injection source. The theoretical curve corresponds to the arithmetic average of the principal components of the diffusivity tensor.

CASE STUDIES

As an example of real microseismicity, we consider a data set of microseismic events that were induced during the 1993 Hot Dry Rock (HDR) experiments performed at the Soultz-sous-Forêts (France) in the upper Rhine valley (Jones et al., 1995). About 25300 m^3 of water were injected into the crystalline rock at a depth of approximately 2920 m. The absolute location error of events was of the order of 20–80 m. The data set contains about 9150 events induced during 379 hours of injection. The cloud of microearthquakes is displayed at the left of Figure 4. The tensor of hydraulic diffusivity in Soultz is characterized by a significant anisotropy with an approximate relation of principal components of 7:19:52 (Shapiro et al., 2003). After scaling the microseismic cloud, the event density can be compared with the distribution predicted by equation 1. The average of the principal components of the hydraulic diffusivity D can then be fitted to match the data. The best-fit curve is shown in Figure 4 at the right. This fit provides an estimate of $D = 0.03$ m^2/s. An excellent agreement of the observed event density with the theoretical curve given by equation 1 is evident.

Independent methods of estimating hydraulic diffusivity at the same location yield similar values: the average principal component of the diffusivity tensor can be computed from results (again based on microseismicity analysis but using completely different features, i.e., fitting of the triggering front) given in Shapiro et al. (1999) to be equal to $D = 0.023$ m^2/s. The estimate of the apparent hydraulic permeability from the same location based on a borehole injection/flow test and reported in Jung et al. (1996) also can be used to compute the hydraulic diffusivity. This approximately yields $D = 0.022$ m^2/s. The microseismicity-based method of estimating hydraulic diffusivity used in Shapiro et al. (1999) provides order of estimates only. The error estimates from this publication are ±50%. The borehole-based estimates characterize the rocks in the vicinity of boreholes. In turn, two additional curves (Figure 4, at the right) corresponding to $D = 0.03 \pm 0.006$ m^2/s show that the uncertainties in the average diffusivity are smaller than ±20%. Therefore, the event-probability–based approach is more precise for characterizing rocks on a kilometer scale than those proposed in Shapiro et al. (1999).

We also applied the new approach to data obtained during fluid-injection experiments at the Fenton Hill HDR site (New Mexico, USA). In 1983, for about 62 hours, more than 21600 m^3 of water were injected into the crystalline rock at a depth of about 3460 m (Fehler et al., 1998). During this time interval, about 9355 events were recorded and located. The accuracy of the locations was better than 100 m (House, 1987). The tensor of diffusivity is characterized by an anisotropy with an approximate relation of the principal components of 2:3:6 (Shapiro et al., 2003). The best fit of analytical function 1 gives an estimate of $D = 0.12$ m^2/s and is shown in Figure 5. Fitting of the triggering front and the back front of seismicity (see Parotidis et al., 2004) provides estimates of $D = 0.14$ m^2/s. A good agreement of these values is evident. Additionally, Figure 5 (at the right) shows two curves with $D = 0.1$ m^2/s and $D = 0.14$ m^2/s, which correspond to ±20% deviation. Three data points in the distance range of 300 to 500 m are located even outside this deviation interval. We explain this by an influence of a strong hydraulic heterogeneity of the medium.

Special attention is required by the third example from the Carthage Cotton Valley gas field (east Texas, USA). In contrast to the previous two case studies concerning crystalline rocks, the Cotton Valley data set was obtained by a hydraulic fracturing of sediments. On May 14, 1997, a hydraulic fracture treatment was performed; for about 7 hours, a total fluid volume of more than 1100 m^3 was injected into sandstones at the depth of 2756–2838 m (Rutledge et al., 2004). The localized 994 microseismic events occurred in the depth range from 2750 to 2850 m (Urbancic et al., 1999). The event location

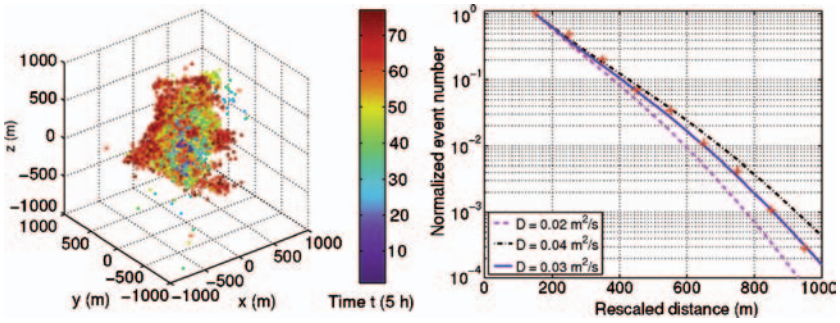

Figure 4. Microearthquakes of the Soultz-sous-Forêts experiment of 1993. (Left) A view of the cloud of seismic events. The colors correspond to the event occurrence time. (Right) Spatial density of the microseismic cloud versus rescaled distance from the injection source (crosses). The lines denote the theoretical distribution given by equation 1.

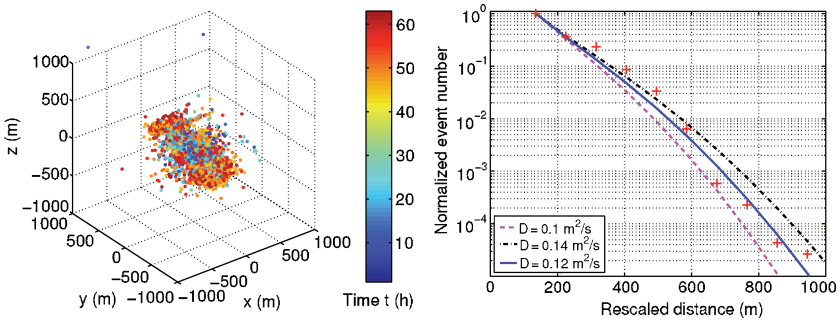

Figure 5. Microearthquakes located in December 1983 during the hydraulic injection into crystalline rock at a depth of 3463 m at Fenton Hill, an HDR site in the USA [for details and further references see Fehler et al. (1998)]. Notations are the same as in Figure 2. (Left) A view of the cloud of seismic events. (Right) Spatial density of the microseismic cloud versus rescaled distance from the injection source.

errors ranged from 14 m near the treatment well to 24 m at the wings of the eastern and western edges of the fracture zones.

In order to discuss this case study in more detail, we show here the distance-versus-time plot for these microearthquakes (Figure 6). Two parabolic curves corresponding to the triggering front $r = \sqrt{4\pi Dt}$ [see Shapiro et al. (2002) for the theory of the triggering front] with two diffusivity estimates ($D = 0.36$ m^2/s and $D = 0.72$ m^2/s) are shown here. The majority of events is located below a parabolic envelope with a diffusivity ranging from $D = 0.36$ m^2/s to $D = 0.72$ m^2/s. A few events occurred relatively far away from the injection source at early times (see the large circles in Figure 6 and Figure 7, at the left). We propose that they were caused by hydraulic fracturing rather than by a diffusive process of pore-pressure relaxation. Probably, a long, thin crack filled with fluid was quickly formed during the first hour of the hydraulic fracturing. This crack has influenced the effective hydraulic properties of the medium. An analysis of the shape of the square-root-occurrence-time–normalized microseismicity cloud of the Cotton Valley (Rentsch, 2003) shows that the diffusivity tensor is characterized by a very strong anisotropy. The approximate relation of principal components is 1:3:46. After the transformation of coordinates, we can analyze event probability (see Figure 7, at the right). Again, we see that the majority of events was triggered by a diffusive process. Between 400- and 500-m distance from the injection source, we observe more events than predicted by equation 1. These outliers correspond to the events that probably occurred during hydraulic fracturing at the very beginning of the injection. The estimation of $D = 0.22$ m^2/s $\pm 20\%$ represents an arithmetic average of the principal components of the effective hydraulic-diffusivity tensor characterizing the seismically active volume of the Carthage Cotton Valley field. The value $D = 0.72$ m^2/s is close to the maximum principal value of the diffusivity tensor.

The resulting diffusivity estimate seems to characterize the medium after the hydraulic fracturing because it is based mainly on the statistics of events occurring after the outliers. The diffusivity anisotropy already reflects the influence of the hydraulically initiated fracture, as well as the influence of lamination of the sedimentary rocks. This well explains strong anisotropy of the diffusivity and its relatively high values, as well as the observation that the largest principal component is approximately horizontal.

Figures 6 and 7 document application of three independent approaches (parabolic envelope, back front, and events density) to the Cotton Valley data set. They all give results of the hydraulic diffusivity in the same order of magnitude. The estimation of the hydraulic diffusivity using the parabolic envelope is based mainly on later events (4.5–9 hours after the injection start) by fitting the outer parabolic boundary of the spatiotemporal distribution. Most events are located below the parabolic envelope on an *r-t* plot. A second signature, the back front, also fits the data after the injection

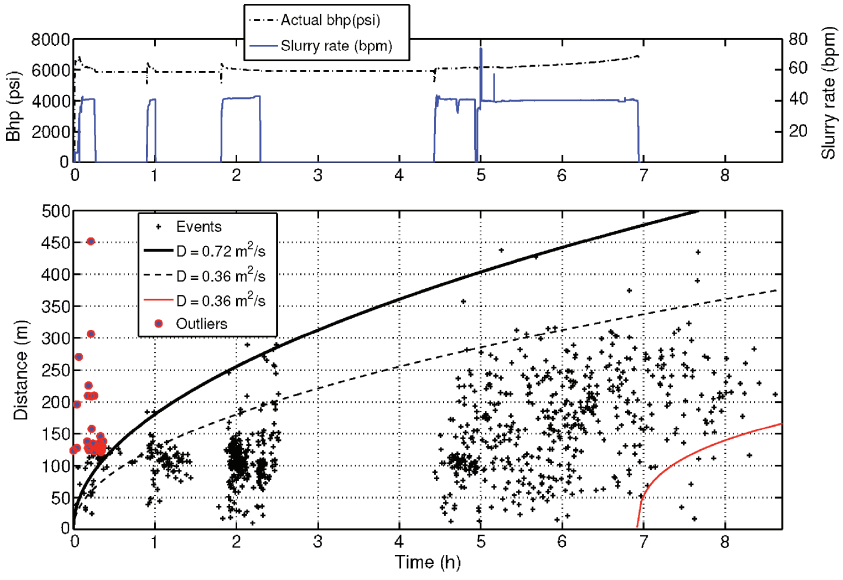

Figure 6. (Top) Actual bottom-hole pressure (psi) and slurry rate (bpm) versus time. (Bottom) Event distance from the injection point versus occurrence time for the Cotton Valley microseimicity. Two black lines show locations of the triggering front for $D = 0.36$ m^2/s and $D = 0.72$ m^2/s. The red line represents the back front for $D = 0.36$ m^2/s. The Cotton Valley diffusivity is characterized by strong anisotropy (Rindschwentner, 2001; Rentsch, 2003). We propose that events denoted by circles above the solid parabolic envelope were triggered by hydraulic fracturing. Data are courtesy of T. Urbancic (ESG).

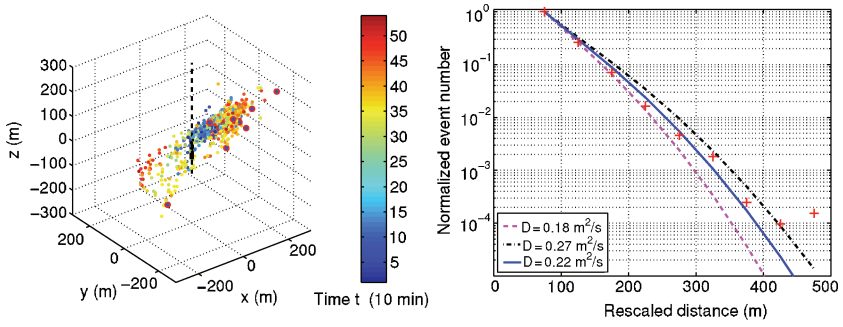

Figure 7. Microearthquakes induced in Cotton Valley field, east Texas, during a fluid injection (hydraulic fracturing) experiment in May 1997. Notations are the same as in Figure 2. (Left) A view of the cloud of seismic events. The large circles correspond to events that are assumed to occur during fracturing. These are the same events as those shown by circles in Figure 6. The solid black line represents the injection interval, and the dashed line, the interpolated treatment well. (Right) Spatial density of the microseismic cloud versus rescaled distance from the injection source.

stop (see the red curve in Figure 6). The seismicity back front describes propagation of the pore-pressure maximum for a boxcar-pressure source of the duration of 6.92 hours. Behind the back front, the triggering of seismicity is very improbable, corresponding to our model. For a detailed description of the back front signature, see Parotidis et al. (2004). The third signature, the event density, considers all events between the injection start and the injection stop. This signature also fits the observed event number per unit volume up to 450-m distance from the injection source (Figure 7). According to these three signatures, it is a reasonable assumption that one of the dominant triggering mechanisms at Cotton Valley was the pore-pressure diffusion. The estimated diffusivity reflects the effective hydraulic diffusivity of the medium. This effective hydraulic diffusivity represents a complex average (upscaling) over the intact rock, the hydraulic fractures, and the hydraulic heterogeneities.

This case study first shows that a plot like that shown in Figure 6 can help to identify events that are probably caused by different triggering mechanisms (e.g., hydraulic fracturing and pore-pressure diffusion). One can expect the diffusion-triggered events to be located mainly below a parabolic envelope of the triggering front. Events that we can identify as hydraulic fracturing events are outliers (early far events located above the triggering front). However, this does not exclude that some events triggered by hydraulic fracturing can be located below the parabolic envelope.

The case study of the Carthage Cotton Valley gas field corresponds to the most complex geologic and technical conditions. It does not comply with our model assumptions in a number of ways: The hydraulic diffusivity is a function of space because of heterogeneity of the medium (e.g., layering). It is also a function of time because it creates a hydraulic fracture. The last process increased the spatial heterogeneity of the diffusivity. Moreover, the fluid entering the hydraulic fracture varied significantly during the period of injection from treated water to a crosslinked gel to a mixture of gel and proppant sand. Finally, Figure 6 shows that the pressure regime was not exactly a nondecreasing function.

Such complexity of the Cotton Valley experiment makes meaningful a very detailed analysis of the relationship between the time-dependent seismicity rate and pressure and flow-rate curves. This analysis is beyond of the scope of our study, the main goal of which is to introduce a new quantitatively interpretable signature of induced microseismicity — the probability of events. However, our analysis of the gross statistics of the microseismicity shows that even for this complex case study, the seismicity statistic can be described by a diffusion-triggering process. The corresponding diffusivity tensor is a rather complex (effective) average of the diffusivity tensor of the propped hydraulic fracture and the heterogeneous diffusivity of the surrounding rocks. It effectively characterizes several processes: the diffusion of fluid pressure in the propped fracture, the leak-off pressure diffusion from the hydraulic fracture into the matrix and natural crack system of the surrounding rocks, and the diffusion of pressure in the rocks. This effective diffusivity should be significantly larger than the diffusivity of the intact rocks; however, it can be proposed as an orientation value for properties of the hydraulic system of the stimulated reservoir after hydraulic fracturing.

DISCUSSION AND CONCLUSIONS

Observations show that clouds of fluid-injection–induced microseismicity require hours or days to reach a size of several hundred meters. This is definitely too slow a process to be described just by the elastic-stress equilibration, which has a characteristic time of elastic-wave propagation (i.e., seconds or less). Our analysis provides additional evidence in favor of the hypothesis that the process of pore-pressure relaxation is at least one of the dominant triggering mechanisms of fluid-induced microseismicity. According to this hypothesis, spatiotemporal distributions of microseismicity are controlled by the hydraulic diffusivity of rocks, as well as by the distribution and degree of rock criticality. We define rock criticality as the minimum pore pressure required at a given location to trigger a seismic event. The criticality of rocks can be described by rather simple statistical models such as a uniform probability-density function. We propose a simple statistical model of the fluid-induced seismicity. Using this model and analyzing three case studies, we have shown that the probability of induced seismic events is well described by the law of pore-pressure relaxation (diffusion; see equation 1 and Figures 4, 5, and 7). Using this observation, we show that the spatial distribution of the density of earthquakes provides a possibility to estimate hydraulic diffusivity on a kilometer scale with high precision. The case study of the Carthage Cotton Valley gas field indicates a way to distinguish seismic events probably triggered by the process of hydraulic fracturing from seismic events triggered by pore-pressure relaxation. For this, an *r-t* plot of the induced seismicity (such as in Figure 6) can be analyzed. Early events that are located clearly above the parabolic envelope of diffusion-triggered earthquakes are proposed to be triggered by hydraulic fracturing. Such a hypothesis could be of great practical importance and requires further detailed study.

The assumptions of our theoretical model are summarized in the section "Statistical model of seismicity triggering." We consider them to be simplifying rather than restrictive assumptions. In reality, hydraulic properties clearly are heterogeneously distributed in rocks. Also, the statistics of seismic criticality can be much more complex than assumed here. We think, however, that the model proposed here correctly reproduces the large-scale picture of the phenomenon, providing us with accurate, scaled-up, effective hydraulic characteristics of rocks. The case studies support the validity of such a conclusion.

It is clear also that explaining the overall statistics of seismicity is not enough to explain triggering mechanisms of all events. Already, the Cotton Valley example indicates at least two important mechanisms at work: hydraulic fracturing and pore-pressure diffusion. Hydraulic heterogeneities and/or heterogeneities of the criticality of the medium can also be of importance. These heterogeneities may exist before injection started. However, they may also be caused by the injection (Rutledge and Phillips, 2002). The corresponding events may be triggered by nonlinear diffusion or a process of tensile opening and propagation of small cracks (Dvorkin and Nur, 1992). Such events can also be found below the envelope of the *r-t* plots. Coupled processes such as thermoporoelastic stress relaxation may also be of significance. Finally, other signatures of seismicity, such as strength of events or fault-plane

solutions, which are not now included in our model, may be included in our future analyses.

ACKNOWLEDGMENTS

Locations and times of seismic events from the Soultz experiment are courtesy of R. Baria and A. Gérard (Socomine). Data of the Fenton Hill experiment are courtesy of M. Fehler (Los Alamos National Laboratory). Data of the Cotton Valley experiment are courtesy of T. Urbancic (ESG) and S. Wolhart (Pinnacle). This work has been supported in part by WIT-university consortium sponsors and in part by Shell.

REFERENCES

Audigane, P., J.-J. Royer, and H. Kaieda, 2002, Permeability characterization of the Soultz and Ogachi large-scale reservoir using induced microseismicity: Geophysics, **67**, 204–211.

Carslaw, H. S., and J. C. Jaeger, 1973, Conduction of heat in solids: Oxford University Press.

Detournay, E., and A. H.-D. Cheng, 1993, Fundamentals of poroelasticity, *in* J. A. Hudson, ed., Comprehensive rock engineering: Principles, practice and projects: Pergamon Press, 113–171.

Dvorkin, J., and A. Nur, 1992, Filtration fronts in pressure compliant reservoirs: Geophysics, **57**, 1089–1092.

Fehler, M., L. House, W. S. Phillips, and R. Potter, 1998, A method to allow temporal variation of velocity in travel-time tomography using microearthquakes induced during hydraulic fracturing: Tectonophysics, **289**, 189–202.

House, L., 1987, Locating microearthquakes induced by hydraulic fracturing in crystaline rocks: Geophysical Research Letters, **14**, no. 9, 919–921.

Jones, R. H., A. Beauce, A. Jupe, H. Fabriol, and B. C. Dyer, 1995, Imaging induced microseismicity during the 1993 injection tests at Soultz-sous-Forets, France: Proceedings of the World Geothermal Congress, 2665–2669.

Jung, R., F. Cornet, F. Rummel, and J. Willis-Richard, 1996, Hydraulic stimulation results 1992/1993, *in* R. Baria, J. Baumgärtner, and A. Gérard, eds., European Hot Dry Rock programme, 1992–1995: Extended Summary of the Final Report to the European Community (DG XII), Contract N JOU2-CT92-0115, 31–41.

Nur, A., and J. Booker, 1972, Aftershocks caused by pore fluid flow?: Science, **175**, 885–887.

Parotidis, M., S. A. Shapiro, and E. Rothert, 2004, Back front of seismicity induced after termination of borehole fluid injection: Geophysical Research Letters, **31**, no. L02612, doi:10.1029/2003GL018987.

Pearson, C., 1981, The relationship between microseismicity and high pore pressures during hydraulic stimulation experiments in low permeability granitic rocks: Journal of Geophysical Research, **86**, 7855–7864.

Rentsch, S., 2003, Hydraulic characterization of rocks using density of induced microseismicity: Master's thesis, Freie Universität Berlin.

Rice, J. R., and M. P. Cleary, 1976, Some basic stress diffusion solutions for fluid-saturated elastic porous media with compressible constituents: Review of Geophysics and Space Physics, **14**, 227–241.

Rindschwentner, J., 2001, Estimating the global permeability tensor using hydraulically induced seismicity: Master's thesis, Freie Universität Berlin.

Rothert, E., and S. A. Shapiro, 2003, Microseismic monitoring of borehole fluid injections: Data modeling and inversion for hydraulic properties of rocks: Geophysics, **68**, 685–689.

Rutledge, J. T., and W. S. Phillips, 2002, A comparison of microseismicity induced by gel-proppant- and water-injected hydraulic fractures, Carthage Cotton Valley gas field, east Texas.: 72nd Annual International Meeting, SEG, Expanded Abstracts, 2393–2396

———, 2003, Hydraulic stimulation of natural fractures as revealed by induced microearthquakes, Carthage Cotton Valley gas field, east Texas.: Geophysics, **68**, 441–452.

Rutledge, J. T., W. S. Phillips, and M. J. Mayerhofer, 2004, Faulting induced by forced fluid injection and fluid flow forced by faulting: An interpretation of hydraulic-fracture microseismicity, Carthage Cotton Valley gas field: Bulletin of the Seismic Society of America, **94**, 1817–1830.

Shapiro, S. A., P. Audigane, and J.-J. Royer, 1999, Large-scale in situ permeability tensor of rocks from induced microseismicity: Geophysical Journal International, **137**, 207–213.

Shapiro, S. A., E. Rothert, V. Rath, and J. Rindschwentner, 2002, Characterization of fluid transport properties of reservoirs using induced microseismicity: Geophysics, **67**, 212–220.

Shapiro, S. A., R. Patzig, E. Rothert, and J. Rindschwentner, 2003, Triggering of seismicity by pore-pressure perturbations: Permeability-related signatures of the phenomenon: PAGEOPH, **160**, 1051–1066.

Trifu, C. I., ed., 2002, The mechanism of induced seismicity: Birkhauser.

Urbancic, T. I., V. Shumila, J. T. Rutledge, and R. J. Zinno, 1999, Determining hydraulic fracture behavior using microseismicity: Vail Rocks '99, 37th U.S. Rock Mechanics Symposium, 991–996.

Van Der Kamp, G., and J. E. Gale, 1983, Theory of earth tide and barometric effects in porous formations with compressible grains: Water Resources Research, **19**, 538–544.

Zoback, M., and H.-P. Harjes, 1997, Injection induced earthquakes and the crustal stress at 9 km depth at the KTB deep drilling site, Germany: Journal of Geophysical Research, **102**, 18477–18492.